

Triassic–Jurassic climate in continental high-latitude Asia was dominated by obliquity-paced variations (Junggar Basin, Ürümqi, China)

Jingeng Sha^{a,1}, Paul E. Olsen^{b,1}, Yanhong Pan^a, Daoyi Xu^c, Yaqiang Wang^a, Xiaolin Zhang^d, Xiaogang Yao^a, and Vivi Vajda^{e,f}

^aState Key Laboratory of Palaeobiology and Stratigraphy, Nanjing Institute of Geology and Palaeontology, Nanjing 210008, China; ^bLamont-Doherty Earth Observatory of Columbia University, Palisades, NY 10968; ^cInstitute of Geology, China Earthquake Administration, Beijing 100029, China; ^dChinese Academy of Sciences Key Laboratory of Crust-Mantle Materials and Environments, School of Earth and Space Sciences, University of Science and Technology of China, Hefei 230026, China; ^eDepartment of Geology, Lund University, 223 62 Lund, Sweden; and ^fDepartment of Palaeobiology, Swedish Museum of Natural History, 104 05 Stockholm, Sweden

Contributed by Paul E. Olsen, January 18, 2015 (sent for review December 19, 2014; reviewed by Linda A. Hinnov and Michael R. Rampino)

Empirical constraints on orbital gravitational solutions for the Solar System can be derived from the Earth's geological record of past climates. Lithologically based paleoclimate data from the thick, coal-bearing, fluvial-lacustrine sequences of the Junggar Basin of Northwestern China (paleolatitude $\sim 60^\circ$) show that climate variability of the warm and glacier-free high latitudes of the latest Triassic–Early Jurassic (~ 198 – 202 Ma) Pangea was strongly paced by obliquity-dominated (~ 40 ky) orbital cyclicity, based on an age model using the 405-ky cycle of eccentricity. In contrast, coeval low-latitude continental climate was much more strongly paced by climatic precession, with virtually no hint of obliquity. Although this previously unknown obliquity dominance at high latitude is not necessarily unexpected in a high CO_2 world, these data deviate substantially from published orbital solutions in period and amplitude for eccentricity cycles greater than 405 ky, consistent with chaotic diffusion of the Solar System. In contrast, there are indications that the Earth–Mars orbital resonance was in today's 2-to-1 ratio of eccentricity to inclination. These empirical data underscore the need for temporally comprehensive, highly reliable data, as well as new gravitational solutions fitting those data.

orbital forcing | obliquity cycle | Triassic–Jurassic | lacustrine sediments | solar system chaos

Our understanding of Triassic and Early Jurassic high-latitude climate, biotic evolution, mass extinction, and geochronology is very poor in contrast to that of the contemporaneous tropics (1, 2). This poor resolution impairs an elucidation of the basic patterns of Earth system function during the early Mesozoic, notably the high-latitude climatic response to orbital forcing, as well as the effects of the eruption of the Triassic–Jurassic Central Atlantic Igneous Province (CAMP) (3). The former issue bears on the stability of the Solar System, in which determining variations in orbital eccentricity (via climatic precession) and inclination (via obliquity) figure as crucial (4–6), and the latter bears on the causes, effects, and recovery from the end-Triassic mass extinction (ETE) (e.g., ref. 2). Here, we describe results of a cyclostratigraphic investigation of lithologic variations in the paleo-high latitude, lacustrine, Late Triassic–Early Jurassic Haojiagou and Badaowan formations of the Junggar Basin, China representing, to our knowledge, the first analysis of orbital cyclicity from a high-latitude, early Mesozoic continental sequence, and a step toward development of an empirical basis for evaluating numerical solutions of Solar System chaotic behavior.

Junggar Basin, Ürümqi, Western China

The thick, nonmarine, early Mesozoic sequence of the Junggar Basin of Western China (Fig. 1 and Figs. S1 and S2) comprises >11 km of largely nonmarine Late Paleozoic to Cenozoic strata deposited in the northwestern-most of the “walled basins” of China (7).

It is a collisional successor basin, established during the Late Permian, 50–75 My after the cessation of subduction and complex amalgamation of microplates and ocean basins. Triassic and Early Jurassic age strata amount to 3,600 m in the interior, subsurface region of the basin (7) but outcrop extensively in several areas. One of the largest outcrops is the Haojiagou section located about 50 km southwest of Ürümqi City on the southern margin of the Junggar Basin of northern Xinjiang Uygur (Uighur) Autonomous Region, Northwestern China (Fig. 1 and Fig. S1) that forms the basis for this report. There, the 1,050 m of the nonmarine Haojiagou and coal-bearing Badaowan formations are continuously exposed and only slightly deformed (Fig. S2). The section has been studied in various aspects (e.g., see *SI Text*), but only one summary on the cyclostratigraphy has been published to date (8).

The paleolatitude of the Junggar Basin for the Triassic–Jurassic is most parsimoniously placed at about 60° N (Fig. 1), constrained by paleomagnetic data (9) interpreted in light of the effects of compaction-induced inclination error (10) and plate-tectonic context (e.g., ref. 7; see *SI Text*). It is the highest latitude continental basin in which Triassic–Jurassic orbitally paced cyclicity has been quantitatively examined.

Significance

Geological records of paleoclimate provide the only constraints on Solar System orbital solutions extending beyond the ~ 50 -Ma limit imposed by chaotic diffusion. Examples of such constraints are coupled high and low latitude, Triassic–Jurassic (~ 198 – 202 Ma) sedimentary cyclicity in coal-bearing outcrops from the $\sim 60^\circ$ N-paleolatitude Junggar Basin (Western China), and contemporaneous tropical basins. Analysis reveals climate variability dominated by obliquity-scale cyclicity in the Junggar Basin and precession-scale cyclicity in the tropics. Together, these geological records empirically constrain orbital solutions by providing joint $g_4 - g_3$ and $s_4 - s_3$ secular frequency estimates of the Earth–Mars orbital resonance. These results demonstrate the opportunity for developing a new class of solutions grounded by geological data extending hundreds of millions of years into the geologic past.

Author contributions: J.S., P.E.O., and D.X. designed research; J.S., P.E.O., Y.P., Y.W., X.Z., X.Y., and V.V. performed research; J.S., P.E.O., D.X., and V.V. analyzed data; P.E.O. wrote the paper; J.S. was the leader of expeditions to Ürümqi and helped write the paper; Y.P., Y.W., X.Z., and X.Y. collected data; and V.V. analyzed samples.

Reviewers: L.A.H., Johns Hopkins University; and M.R.R., New York University.

The authors declare no conflict of interest.

Freely available online through the PNAS open access option.

¹To whom correspondence may be addressed. Email: polsen@ldeo.columbia.edu or jgsha@nigpas.ac.cn.

This article contains supporting information online at www.pnas.org/lookup/suppl/doi:10.1073/pnas.1501137112/-DCSupplemental.

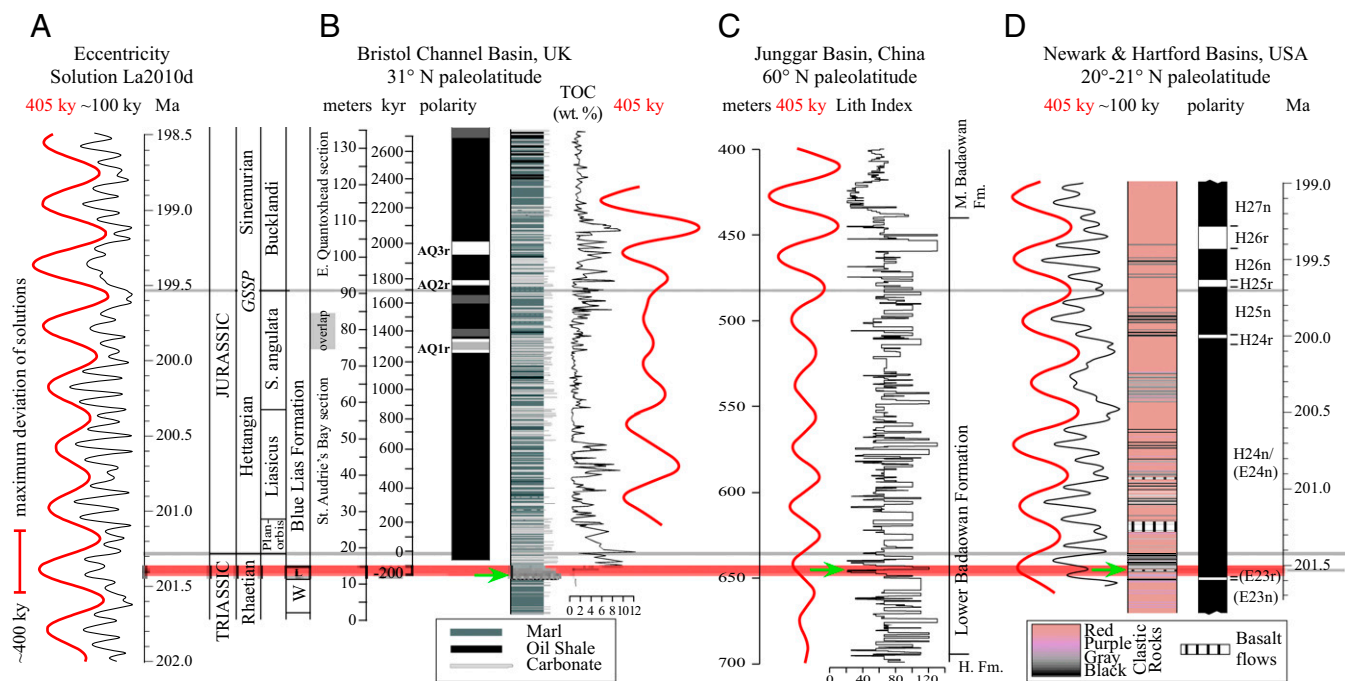


Fig. 2. LITH Index data (C) and correlative sections: (A) Laskar 2010d solution (21); (B) Bristol Channel (United Kingdom); (C) Junggar Basin (China); (D) the Newark–Hartford astrochronology and geomagnetic polarity time scale (APTS). The thick red bar indicates the interval of extinctions and uncertainty of correlations between the sections, and the green arrows indicate the last appearance of *L. rhaeticus* (SI Text). A and B are adapted from refs. 19 and 31 (potential error added from ref. 21); D is modified from refs. 25 and 26. Note the difference in phase between the phasing eccentricity cycles in the La2010d solution (selected by ref. 31 for comparison with B) and the geological data that we attribute to chaotic drift; therefore, we have retained the independent times scales for both A and D.

the middle of the 20- to 40-m range of the fluctuating band of high amplitude in the wavelet spectra (Fig. 4 and Fig. S4).

Assuming that we have correctly identified the 405-ky cycle in the LITH index depth series, the most prominent higher frequency cycles of the Haojiagou and lower Badaowan formations have spectral peaks with periods of between 30 ky and 60 ky, with the median periods most strongly at 42.5 and 44.6 ky. These periods are close to what would be expected for the obliquity periods, which for the Triassic–Jurassic should be 36.6 and 46.7 ky (6, 27, 28), assuming a constant rate of recession of the moon and constant dynamic ellipticity of the Earth, with the former period being of much higher magnitude. The shift to lower frequencies from the expected precession and obliquity periods is also observed in the precession band in the eastern North American Triassic Locketong Formation where the shift has been interpreted as a consequence of accumulation rate variability (22, 24). The most dramatic expression of such a frequency-modulated shift would be occasional and perhaps periodically spaced hiatuses as might be present in the fluvial portions of the Junggar sequences. However, it is not impossible that the unexpectedly low frequencies could be real, caused by nonlinear changes through time in dynamic ellipticity that could produce occasional decreases in precession rate (20, 29). Nonetheless, because the independently U–Pb–calibrated (2) periods of Newark Basin latest Triassic–Early Jurassic precession-band cycles are compatible with an average period of about 20 ky, spectral distortion from frequency modulation is the simpler explanation for the apparent discrepancy. Relatively less important in the analysis are periods that could be assigned to climatic precession although significant periods are present in the MTM analyses. The weakness in amplitude at precessional periods could be a real feature of the climate system of the Mesozoic (see *Mesozoic High- vs. Low-Latitude Cyclicity*) or it could be due to accumulation rate noise at the precessional frequencies. Periods at about 100 ky, although present, are weak, consistent with the low power of the assumed precession

periods, but, because we seem to be able to recognize the 405-ky cycle, some climatic precession signal is evidently present.

Based on our analysis of thickness periodicities, the sedimentary cycles attributed to climatic precession, obliquity, and eccentricity cycles correspond to the microcycles and different scales of mesoscale cycles of Hornung and Hinderer (14). These Junggar Basin strata are similar to what Olsen and Kent (30) termed Kap Stewart-type lacustrine sequences, named after the eponymous gray and black cyclical strata of Jamesonland East Greenland (16). We propose that the cycles in these sequences fit into a continuum of orbitally forced lacustrine sedimentary cycles extending from the tropics to the high latitudes, with the Haojiagou and Badaowan cycles in Kap Stewart-type lacustrine sequences representing the humid high latitude end member of the cyclicity (30). This type of lacustrine sequence and cycles may well extend to the paleo-north pole, for which there is obviously no sedimentary analog today.

Testing the Junggar Basin Age Model

Direct age calibration of the section by radiometric or paleomagnetic means does not yet exist for the Triassic–Jurassic of the Junggar Basin; however, the age model may be at least partially tested by its consistency with contemporaneous records from elsewhere, specifically the Newark–Hartford basins of eastern North America, the Bristol Channel Basin of the United Kingdom, and the Pucara Basin of Peru (Fig. 1, Fig. S3, and Table 1).

To compare the obliquity-dominated successions of the Junggar Basin with the precession-dominated eastern North American lacustrine sequences and the contemporaneous marine section at St. Audrie’s Bay in the United Kingdom (Bristol Channel Basin), we compared the filtered 405-ky cycle from the three sections (SI Text) and correlated them using the last appearance of *Lunatisporites rhaeticus* (green arrows in Fig. 2). Using the latter datum results in the encouraging observation that the 405-ky cycles are in phase and that the interval of low

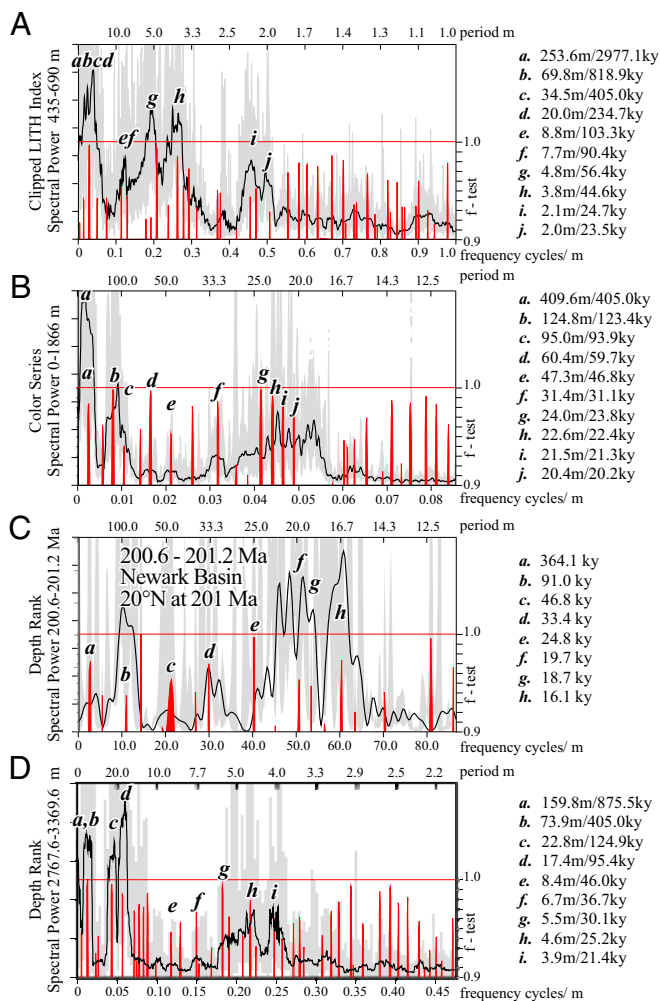


Fig. 3. MTM spectra from high and low Triassic–Jurassic latitudes: (A) high-latitude Badaowan Formation, Junggar Basin, China; (B) contemporaneous low-latitude Portland Formation, Hartford Basin, eastern United States; (C) contemporaneous low-latitude Newark Basin Towaco and Boonton formations, eastern United States; and (D) equatorial Lockatong Formation, Newark Basin, eastern United States (modified from ref. 22), showing that the low-latitude low obliquity signal is not limited to the Triassic–Jurassic boundary interval. Spectra are lined up by time based on the 405-ky cycle. Highlighted spectral peaks are only those with both high amplitude and high *f*-test significance (>0.9) (red). The area between the upper and lower confidence limits is shaded gray. Note that, for A, B, and D, accumulation rate is based on setting a specific spectral peak to 405 ky whereas, in C, accumulation rate is derived from U–Pb dates and tuning to a 20-ky average climatic precession cycle (2). See *SI Text* for details.

variance interpreted as a minimum in the long eccentricity $g_4 - g_3$ cycle (2, 19, 31) occurs in same relative position (Fig. 2).

The Newark–Hartford astronomical calibration was independently corroborated using U–Pb dates from interbedded lavas (2) and could be confidently and tightly correlated to marine sections. Tying the Newark–Hartford and Bristol Channel Basin astrochronologies at the biostratigraphic ETE with a U–Pb–determined age of its base at 201.564 ± 0.015 Ma (2) (from the Newark–Hartford section) provided near perfect agreement between the magnetostratigraphy of the two areas, as well as with the astrochronological ages of the Hettangian–Sinemurian boundary, the formal definition of which (GSSP, global boundary stratotype section and point) is within the Bristol Channel sequence (31) (Table 1). The Pucara Basin section contains multiple dated ashes (ref. 17 and references therein, allowing further testing of the

astrochronologies, with the marine ammonite-based ETE and Hettangian–Sinemurian boundary in complete agreement (within tight error) with the Newark–Hartford and Bristol Channel astrochronologies (Fig. 2 and Table 1). This framework of multiple independent constraints strongly supports the Junggar Basin astrochronology.

Mesozoic High- vs. Low-Latitude Cyclicity

The Haojiagou and Badaowan formations are, to our knowledge, the first high-latitude early Mesozoic continental sequences for which astronomical forcing has been quantitatively explored, and, unlike contemporaneous lower-latitude analyses, obliquity-paced cyclicity is a dominant high-frequency component of the variability. A comparison of MTM spectra and wavelet spectra from the high-latitude Badaowan Formation and the lower latitude continental sequences in eastern North America shows this difference dramatically (Fig. 4). The lower latitude records for both Triassic and Jurassic have little obliquity signal and are strongly dominated by climatic precession corroborated by the independent U–Pb and magnetostratigraphic tests (2, 31) (Fig. 2 and Table 1).

Obliquity-related insolation variation is greatest at high latitudes, but dominance of obliquity in climate is not necessarily expected as a consequence. In theory, interannual insolation forcing at a given calendar day or yearly average is dominated by precessional cycles at all latitudes, even at the poles where the obliquity effect on insolation variation is the greatest (32). However, obliquity dominance in high-latitude climate is by no means without precedent, the most spectacular example of which is the dominance of 41-ky glacial cycles of all but the last 0.8 million y (3.0–0.8 Ma) of the Neogene (33) and is also an important component of variability in the high-latitude (~ 52 – 55° N) Lake Baikal sedimentary record (34) situated at a similar latitude to the Junggar Basin deposits.

Differences between the Late Neogene world and that of the Triassic–Jurassic are vast, including but not limited to continental

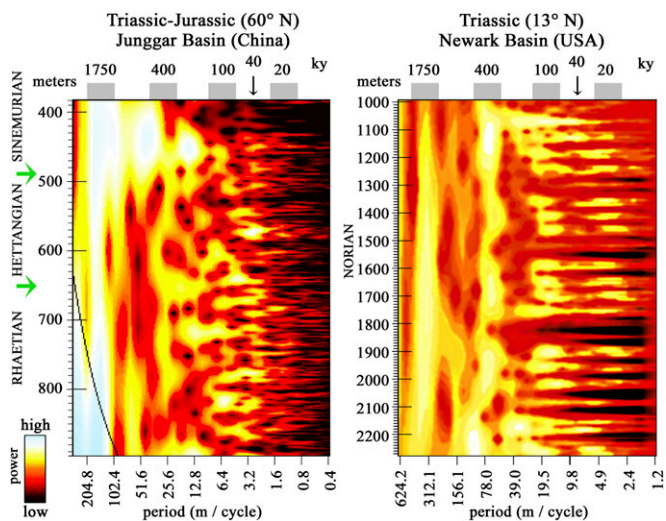


Fig. 4. Untuned (depth) wavelet spectra of the LITH data of high-latitude Haojiagou and Badaowan formations of Rhaetian to Sinemurian age (Late Triassic–Early Jurassic, Junggar Basin) with strong power in the obliquity band (~ 40 ky) and low power in the climatic precession (~ 20 ky) band compared with the low-latitude Lockatong Formation of Norian (depth rank, Late Triassic, Newark Basin) (from ref. 28). Spectra are lined up along the frequency modulations (in thickness) of the 405-ky cycle. Similar continuous data for the Rhaetian–Sinemurian of eastern North America are not available. Lower and upper green arrows for the Junggar Basin indicate the end-Triassic extinction (201.6 Ma) and the Hettangian–Sinemurian boundary (199.7 Ma), respectively (Figs. S3 and S4).

Table 1. U-Pb and astrochronological ages compared

Boundary or unit	Newark igneous*	Newark–Hartford*	Pucara Basin	Bristol Channel† Pucara‡/Newark§
Hettangian–Sinemurian boundary	—	199.70 ± 0.02	199.46 ± 0.17	199.61/199.66
Hook Mountain Basalt	200.916 ± 0.064	200.93 ± 0.02	—	—
Preakness Basalt	201.274 ± 0.032	201.28 ± 0.02	—	—
Rhaetian–Hettangian boundary	—	201.42 ± 0.022	201.36 ± 0.14‡	201.32/201.37
Orange Mountain Basalt	201.520 ± 0.034	201.52 ± 0.02	—	—
End-Triassic extinction	201.564 ± 0.015	201.56 ± 0.02	201.51 ± 0.15	201.51/201.56

*See ref. 2 for ages. Details in Table S2.

†See refs. 19 and 31 for ages. Details in Table S2.

‡See refs. 12 and 17 for ages. Details in Table S2.

§See ref. 15 for ages. Details in Table S2.

configuration with Pangea straddling the equator, a lack of polar glaciers (35), and very high CO₂ (approximate background at between 1,000 and 2,000 ppm and maxima of >6,000 ppm) (36)—a world without modern analog. Therefore, explanations of obliquity dominance due to fluctuations of high-latitude glaciers are difficult to support for the early Mesozoic. However, some aspects of these explanations might still be pertinent to the Haojiagou and Badaowan formations. In particular, integrated summer insolation is directly controlled by obliquity and has been proposed as a cause of the late Neogene obliquity dominance in glacial fluctuations (32), and it is possible that the highly vegetated Triassic–Jurassic high latitudes were similarly sensitive to the length of the growing season and associated timing and magnitude of precipitation and evaporation.

Implications for Chaotic Evolution of the Solar System and Astronomical Solutions

Since Poincaré's (37) contribution to dynamical systems, it has been recognized that the Solar System has chaotic properties. Chaos significantly limits the accuracy of numerical solutions of planetary behavior, including the frequency and phases of climatically important orbital cycles (4–6), and impedes understanding of the general problem of the stability of the Solar System (5, 13). At time scales of hundreds of millions of years, chaotic diffusion of the gravitational system of the Solar System results in an inability to recognize accurate solutions of planetary orbital and axial behavior (4).

Integral to the long-term chaotic behavior of the Solar System are the secular resonances of the planets, particularly for the inner Solar System. Particularly important are those of Earth and Mars (4), affecting modulations of eccentricity and obliquity with present periods of 2.4 and 1.2 My ($g_4 - g_3$ and $s_4 - s_3$, respectively, where g_4 and g_3 are related to the precession of the orbital perihelia of Mars and Earth and s_4 and s_3 are related to orbital inclination). However, due to chaotic diffusion of the gravitational system, these periods are expected to change through time. Presently, there is a two-to-one ratio of the eccentricity modulator (2.4 My) to the obliquity modulator (1.2 My), reflecting the secular resonant argument $2(s_4 - s_3) - (g_4 - g_3) = 0$, which is currently in libration. However, there are expected to be important transitions in the chaotic behavior of the gravitational system from libration to circulation so that the eccentricity and obliquity modulators are equal ($s_4 - s_3) - (g_4 - g_3) = 0$ (38). Because both the period and state of these modulating cycles have varied in an unknown way in deep time, strict interpretation of insolation curves are unreliable beyond about 50 Ma (20, 21). This uncertainty is most obviously reflected in the eccentricity and obliquity modulating cycles with periods longer than 405 ky and the long-term phase relationships of all of the cycles. Without geological data with a long obliquity record, it is not possible to determine when these transitions in the Earth–Mars resonances

occur or even if they occur, or what the periods of the long eccentricity or inclination cycles should be.

In addition to being a celestial mechanical problem, chaotic drift in the gravitational solutions also poses fundamental Earth science problems because it limits tuning of geological records to insolation curves and our ability to use astrochronologies to assess and improve the accuracy of important isotopic dating systems (e.g., ref. 39). Empirical, deep-time geological data have the potential to allow us to determine which solutions best fit the actual history of the Solar System.

To quantify the actual behavior of the celestial mechanical gravitational system, precession-related (eccentricity) and obliquity-related cycles need to be isolated in geological records. Continental records, which tend to be tightly coupled to local forcing, provide a possible mechanism to isolate precession-related eccentricity cycles, dominant at low latitudes, from the obliquity-related cyclicity important at higher latitudes.

Previous quantitative investigations of long Late Triassic–Early Jurassic records have been limited to the lower latitudes, largely the tropics and subtropics in eastern North America (2, 22, 24, 25) and the United Kingdom (e.g., refs. 19 and 40). In these areas (20°–30° N) (10), the effects of obliquity on local climate forcing would be expected to be small compared with the higher latitudes, as predicted by basic astronomical theory, although precessional effects should always be greatest in insolation at all latitudes, and that is what is observed for the Triassic–Jurassic in the records described thus far. In the case of the tropical records in eastern North America, obliquity was barely detected (22, 24), but a strong 1.6- to 1.8-My cycle in eccentricity ($g_4 - g_3$) is present, differing from the present 2.4 My presumably because of chaotic diffusion (6, 24). More or less the same value of the $g_4 - g_3$ cycle, in the same phase, is present in the contemporaneous tropical pelagic cherts from the Panthalassic Ocean at Inuyama, Japan (41).

Until now, there have been no long Triassic–Jurassic, high-latitude records that have been quantitatively analyzed, and therefore we have had little knowledge of what the quantitative obliquity behavior was, especially with regard to their modulating cycles. Importantly, there is a strong suggestion of modulation of the obliquity by an ~819-ky (~70-m) cycle in the upper Haojiagou and lower Badaowan, visible in the wavelet spectrum (Fig. 3 and Fig. S4) where it is evident as a modulation in the strength of obliquity cycle (Fig. S4), both as filtered and demodulated data (Figs. S5–S7), and also as period in its own right (Fig. S4). This period is missing or extremely weak in the tropical continental records (22, 24). Together, the data from the Junggar Basin, Newark–Hartford basins, and St. Audrie's Bay section suggest the present-day two-to-one ratio (Early Jurassic, ~1.6–0.8 My) of orbital eccentricity to inclination for the state of the Earth–Mars resonance, but with different periods and phases not seen in existing orbital solutions (21) (Fig. 2).

Conclusions

Analysis of the LITH proxy of environmental change shows that an astronomical signal in which obliquity is dominant can be extracted from lacustrine strata of the high-latitude ($\sim 60^\circ$ N) Junggar Basin straddling the end-Triassic extinction and Triassic–Jurassic boundary. Constrained by fixing the accumulation rate to the 405-ky eccentricity cycle, data show that the main periods of obliquity for the Late Triassic–Early Jurassic are present and were dominant components of high-latitude Early Mesozoic climate, dramatically different from the climatic precession-dominated continental tropics. In combination, the data are incompatible with published astronomical solutions for the Triassic–Jurassic in phase and amplitude, consistent with chaotic behavior of the Solar System whereas, at the same time, the Earth–Mars orbital resonance seems to have been in today’s two-to-one ratio of eccentricity to inclination, providing a constraint for the Earth–Mars secular resonance for around 201 Ma. With the prospect of the acquisition of better temporally resolved records from deeper lake settings in the Junggar and other basins, the use of more directly climate-sensitive proxies, and additional exploration of the paleobiological context of the strata, it will be possible to test these findings, constraining the history of Solar System chaos, during this transitional time in Earth history.

Methods

LITH index data were recorded during the 1996, 1998, and 2008 field seasons using standard descriptive field methods. Standard preparation procedures were used to prepare the palynological slides, archived at the Department of Geology, Lund University, Sweden. The evolutive FFT and MTM spectra were developed using Analyseries (2.0) (42), and the evolutive wavelet spectra were computed using the Matlab script of Torrence and Compo (43). See *SI Text* for additional methodological details.

ACKNOWLEDGMENTS. We thank Deng Shenghui for helpful comments in the field and on the manuscript and Dennis Kent for help in interpreting the paleolatitude of the basin. We are grateful to Ji Xuefeng and Cheng Xiansheng, who guided us in fieldwork and shared significant unpublished information. We thank Christopher Scotese for help in producing the reconstruction of Pangea in Fig. 1. The manuscript was reviewed by Linda Hinnov and Michael Rampino, who provided many useful suggestions. Research was supported by the National Basic Research Program of China (973 Program 2012CB821906), the Strategic Priority Research Program (B) (Chinese Academy of Sciences XDB03010101), National Natural Science Foundation of China (91114201), Bureau of Geological Survey of China, the National Committee of Stratigraphy of China, and the Linnaeus Centre, Lund University Carbon Cycle Centre (LUCCI) funded through the Swedish Research Council (349-2007-8705). This article is a contribution to United Nations Educational, Scientific and Cultural Organization–International Union of Geological Sciences–International Geoscience Programme (UNESCO-IUGS-IGCP) Project 632.

- Irmis RB, Whiteside JH (2010) Newly integrated approaches to studying Late Triassic terrestrial ecosystems. *Palaios* 25:689–691.
- Blackburn TJ, et al. (2013) Zircon U–Pb geochronology links the end-Triassic extinction with the Central Atlantic Magmatic Province. *Science* 340(6135):941–945.
- Marzoli A, et al. (1999) Extensive 200-million-year-old continental flood basalts of the central Atlantic magmatic province. *Science* 284(5414):616–618.
- Laskar J (1999) The limits of Earth orbital calculations for geological time-scale use. *Phil Trans R Soc Lond A* 357(1757):1735–1759.
- Laskar J (2013) Is the Solar System stable? *Chaos* 2013:239–270.
- Hinnov LA (2013) Cyclostratigraphy and its revolutionizing applications in the earth and planetary sciences. *Geol Soc Am Bull* 125(11–12):1703–1734.
- Carroll AR, Graham SA, Smith ME (2010) Walled sedimentary basins of China. *Basin Res* 22(1):17–32.
- Sha J, et al. (2010) Astronomical calibrated time intervals for the non-marine Badaowan Formation, Lower Jurassic in Hajojiagou of Ürümqi City, Western China. *Earth Sci Front* 17(Special Issue):22–23.
- Choulet F, et al. (2013) First Triassic palaeomagnetic constraints from Junggar (NW China) and their implications for the Mesozoic tectonics in Central Asia. *J Asian Earth Sci* 78:371–394.
- Kent DV, Tauxe L (2005) Corrected Late Triassic latitudes for continents adjacent to the North Atlantic. *Science* 307(5707):240–244.
- Willis KJ, McElwain JC (2002) *The Evolution of Plants* (Oxford Univ Press, New York).
- Gueex J, et al. (2012) Geochronological constraints on post-extinction recovery of the ammonoids and carbon cycle perturbations during the Early Jurassic. *Palaeogeogr Palaeoclimatol Palaeoecol* 346–347:1–11.
- van Vugt N, Langereis CG, Hilgen FJ (2001) Orbital forcing in Pliocene–Pleistocene Mediterranean lacustrine deposits: Dominant expression of eccentricity versus precession. *Palaeogeogr Palaeoclimatol Palaeoecol* 172:193–205.
- Hornung J, Hinderer M (2011) Depositional dynamics and preservation potential in a progradational lacustrine fluvio-deltaic setting: Implications for high-resolution sequence stratigraphy (Upper Triassic, Northwestern China). *From River to Rock Record: The Preservation of Fluvial Sediments and Their Subsequent Interpretation*, eds Davidson SK, Leleu S, North CP (SEPM Society for Sedimentary Geology, Tulsa OK), SEPM Special Publication No. 97, pp. 281–310.
- Whiteside JH, et al. (2011) Pangean great lake palaeoecology on the cusp of the end-Triassic extinction. *Palaeogeogr Palaeoclimatol Palaeoecol* 301(1–4):1–17.
- Dam G, Surlyk F (1992) Forced regressions in a large wave-dominated and storm-dominated anoxic lake, Rhaetian–Sinemurian Kap Stewart Formation, East Greenland. *Geology* 20:749–752.
- Wotzlav J-F, et al. (2014) Towards accurate numerical calibration of the Late Triassic: High-precision U–Pb geochronology constraints on the duration of the Rhaetian. *Geology* 42:571–574.
- Whiteside JH, Olsen PE, Eglinton T, Brookfield ME, Sambrotto RN (2010) Compound-specific carbon isotopes from Earth’s largest flood basalt eruptions directly linked to the end-Triassic mass extinction. *Proc Natl Acad Sci USA* 107(15):6721–6725.
- Ruhl M, et al. (2010) Astronomical constraints on the duration of the early Jurassic Hettangian stage and recovery rates following the end-Triassic mass extinction (St. Audrie’s Bay/East Quantoxhead, UK). *Earth Planet Sci Lett* 295:262–276.
- Laskar J, et al. (2004) A long-term numerical solution for the insolation quantities of the Earth. *Astron Astrophys* 428:261–285.
- Laskar J, Fienga A, Gastineau M, Manche H (2011) La2010: A new orbital solution for the long-term motion of the Earth. *Astron Astrophys* 532:A89.
- Olsen PE, Kent DV (1996) Milankovitch climate forcing in the tropics of Pangea during the Late Triassic. *Palaeogeogr Palaeoclimatol Palaeoecol* 122:1–26.
- Kent DV, Olsen PE (1999) Astronomically tuned geomagnetic polarity time scale for the Late Triassic. *J Geophys Res* 104:12,831–12,841.
- Olsen PE, Kent DV (1999) Long-period Milankovitch cycles from the Late Triassic and Early Jurassic of eastern North America and their implications for the calibration of the early Mesozoic time scale and the long-term behavior of the planets. *Philos Trans R Soc Lond* 357:1761–1787.
- Whiteside JH, Olsen PE, Kent DV, Fowell SJ, Et-Touhami M (2007) Synchrony between the CAMP and the Triassic–Jurassic mass-extinction event? *Palaeogeogr Palaeoclimatol Palaeoecol* 244(1–4):345–367.
- Kent DV, Olsen PE (2008) Early Jurassic magnetostratigraphy and paleolatitudes from the Hartford continental rift basin (eastern North America): Testing for polarity bias and abrupt polar wander in association with the central Atlantic magmatic province. *J Geophys Res* 113:B06105.
- Berger A, Loutre MF, Laskar J (1992) Stability of the astronomical frequencies over the Earth’s history for paleoclimate studies. *Science* 255(5044):560–566.
- Olsen PE, Whiteside JH (2008) Pre-Quaternary Milankovitch cycles and climate variability. *Encyclopedia of Paleoclimatology and Ancient Environments*, Earth Science Series, ed Gornitz V (Kluwer Academic Publishers, Dordrecht, The Netherlands), pp 826–835.
- Morrow E, Mitrovica JX, Forte AM, Glišović P, Huybers P (2012) An enigma in estimates of the Earth’s dynamic ellipticity. *Geophys J Int* 191:1129–1134.
- Olsen PE, Kent DV (2000) High resolution early Mesozoic Pangean climatic transect in lacustrine environments. *Epicontinental Triassic, Volume 3*, eds Bachmann G, Lerche I (Zentralblatt für Geologie und Paläontologie VIII) (Schweizerbart Science Publishers, Stuttgart), pp 1475–1496.
- Hüsing SK, et al. (2014) Astronomically-calibrated magnetostratigraphy of the Lower Jurassic marine successions at St. Audrie’s Bay and East Quantoxhead (Hettangian–Sinemurian; Somerset, UK). *Palaeogeogr Palaeoclimatol Palaeoecol* 403:43–56.
- Huybers P (2006) Early Pleistocene glacial cycles and the integrated summer insolation forcing. *Science* 313(5786):508–511.
- Raymo ME, Nisancioglu K (2003) The 41kyr world: Milankovitch’s other unsolved mystery. *Paleoceanography* 18:PA1011.
- Prokopenko AA, Hinnov LA, Williams DF, Kuzmin MI (2006) Orbital forcing of continental climate during the Pleistocene: A complete astronomically tuned climatic record from Lake Baikal, SE Siberia. *Quat Sci Rev* 25:3431–3457.
- Frakes LA, Francis JE, Sykyus JL (1992) *Climate Modes of the Phanerozoic* (Cambridge Univ Press, Cambridge, UK).
- Schaller MF, Wright JD, Kent DV (2011) Atmospheric PCO₂ perturbations associated with the Central Atlantic Magmatic Province. *Science* 331(6023):1404–1409.
- Poincaré H (1892–1899) *Les Méthodes Nouvelles de la Mécanique Céleste* (Gauthier-Villars, Paris), Vol I–III, reprinted by Blanchard, 1987.
- Laskar J (2003) Chaos in the Solar System. *Ann Henri Poincaré* 4(Suppl 2):S693–S705.
- Kuiper KF, et al. (2008) Synchronizing rock clocks of Earth history. *Science* 320(5875):500–504.
- Kemp DB, Coe AL (2007) A nonmarine record of eccentricity forcing through the Upper Triassic of southwest England and its correlation with the Newark Basin astronomically calibrated geomagnetic polarity time scale from North America. *Geology* 35(11):991–994.
- Ikedo M, Tada R (2013) Long period astronomical cycles from the Triassic to Jurassic bedded chert sequence (Inuyama, Japan): Geologic evidences for the chaotic behavior of solar planets. *Earth Planets Space* 65:351–360.
- Paillard D, Labeyrie L, Yiou P (1996) Macintosh program performs time-series analysis. *Eos Trans AGU* 77:379.
- Torrence C, Compo GP (1998) A practical guide to wavelet analysis. *Bull Am Meteorol Soc* 79:61–78.

Supporting Information

Sha et al. 10.1073/pnas.1501137112

SI Text

Paleogeographic Reconstruction. The illustration of Pangea in Fig. 1 and Fig. S1 was redrafted from a reconstruction for the Triassic–Jurassic transition (201.6 Ma) produced by the PALEOMAP Project (1–3) displayed using GoogleEarth. The positions of the Pucara (Peru), Newark–Hartford (United States), Bristol Channel (United Kingdom), and Junggar (Western China) basins on Pangea were then translated as rigid plate south about 3° along the prime meridian to bring their paleolatitude into agreement with ref. 4. This slight reconfiguration produced virtually no change in the latitude of the Junggar Basin at about 60° N from the PALEOMAP reconstruction.

A 60° paleolatitude for the Junggar is in agreement with several additional lines of evidence. Paleomagnetic determinations of paleolatitude of Triassic–Jurassic strata from Junggar and the adjacent Tarim Basin (e.g., ref. 5), although scarce and wholly from sedimentary rocks, suggest a paleolatitude close to that of the present 45° N. The existing paleomagnetic literature, however, does not take into account the effects of compaction-induced inclination error (4, 6, 7), which is greatest at the latitudes suggested by Carroll et al. (8) for the Junggar Basin. Correcting for paleomagnetic inclination error has proved crucial in reconciling discrepant igneous and sedimentary paleomagnetic data in Eastern North America and Greenland (6) in strata correlative to those discussed here, and an approximate correction of 10–15° of paleolatitude is plausible for the Junggar Basin, an estimate of which can be tested by the collection of additional paleomagnetic data. Carroll et al. (8) show similarly high latitude for the basin (~60° N) based on the plate-tectonic context. The estimated position of 60° N as shown in the PALEOMAP reconstructions is therefore plausibly the best available estimate of latitude (Fig. 1).

Location of the Haojiagou Section. The Haojiagou and Badaowan formations outcrop more or less continuously in badlands along the Haojiagou (gou = valley) located at about 50 km southwest of Ürümqi City on the southern margin of the Junggar Basin of the northern Xinjiang Uygur (Uighur) Autonomous Region, Northwestern China (Figs. 1 and 2 and Figs. S1 and S2). About 1,100 m of this section is the basis of this report, beginning at ~43° 38.452' N, 87° 13.266' E and ending 43° 39.889' N, 87° 12.170' E. The section has been studied in various aspects (e.g., refs. 9–16), but only one summary on the cyclostratigraphy has been published to date (17). The data presented here were collected on the east side of the valley.

Construction of the LITH Index. The Haojiagou section was described by Deng et al. (18), with the lithologic data being collected and obtained during fieldwork in 1996, 1998, and 2008. The initial analysis is distinguished by the thickness and lithologic features, reflecting the paleoenvironment, of each measured layer. By using the semiquantitative classification of lithology called the “LITH” index (19), a hierarchy of cycles based on sedimentary rock types was recognized, and the different digital numbers (LITH values) were defined for various rock types (Table 1). The variations (values between 10 and 130) in LITH produce the obvious cyclicity. We converted two measurements (depth measurements and LITH measurement), by interpolating a LITH value at 0.1-m intervals within each layer, into a numerical time series forming a new time series, LITH time series, on which our times series analyses were performed (Fig. S3).

Temporal Constraints on the Junggar Latest Triassic and Earliest Jurassic Strata. Forty samples spanning the boundary of the Haojiagou and Badaowan formations, Junggar Basin, China were examined for palynology. Of these samples, 35 were usefully productive samples (Fig. S3) and formed the basis of the range chart shown in Fig. 3. Our analysis focuses on the ETE, supercedes the palynological analysis in Sha et al. (15), and includes more samples for higher resolution. Samples were processed at Global GeoLab Ltd., Canada (www.globageolab.com) following standard methods. The palynological slides and residues are stored at the Department of Palaeobiology, Swedish Museum of Natural History.

The sedimentary successions of the Haojiagou and Badaowan formations at the Haojiagou section yielded well-preserved miospore assemblages of medium diversity; 60 species of fossil pollen and spore taxa were identified in this study, together with a putative dinoflagellate (*Chytroeisphaeridia* sp.) and the chlorophyte (green alga) *Botryococcus braunii*. The age assessment is based on a combination of last and first appearance datums for key taxa (Fig. S3). Typical Triassic elements persist up to bed 52, including *Lunatisporites rhaeticus* and *Limboisporites* spp., whereas the abundant occurrence of *Retritriletes semimuris* and *Retritriletes austroclavatidites* in bed 53 suggests a Hettangian age (20), and the end of the ETE interval (Fig. 3 and Fig. S3).

The presence of *Cerebropollenites macroverrucosus* and *Calialasporites trilobatus* in bed 81 suggests a Sinemurian–Pliensbachian age (21) for that level. The comparison with European and Australian palynostratigraphical schemes is tentative because these regions represent different floral paleo-provinces from those previously described for this region (9, 12) and because correlative zonation schemes between the regions have not been erected. Identification of the Hettangian–Sinemurian boundary to the Haojiagou section is more problematic because there is apparently no change in sporomorph composition across that boundary at the base-Sinemurian GSSP in the United Kingdom or Europe in general (22–24).

Thus, based on the palynology, we have placed the top of the extinction interval, still in the late Rhaetian, at the last appearance datum (LAD) of the taeniate gymnosperm pollen *L. rhaeticus*. This sporomorph is regarded as a near-end-Rhaetian marker in Europe (including the United Kingdom), Greenland, and Eastern North America (25–29), where its last appearance occurs close to and above the initial expression of the end-Triassic extinction. In Eastern North America, the last appearance of this pollen taxon occurs in strata about 60 ky younger than the initiation of the initial ETE, as constrained by both U-Pb dates and astrochronology (30), and the Triassic–Jurassic boundary occurs about 40 ky after that based on extrapolation and correlation with United Kingdom sections (31). Thus, we use the LAD of *L. rhaeticus* as a tie point to pin the ETE within the studied successions (Figs. 2 and 3).

In terms of floral provinces, Sun et al. (ref. 13 and references therein) argue that the Haojiagou (Late Triassic) floral assemblage belongs to the *Danaeopsis–Symopteris* assemblages [updated from the original *Danaeopsis–Bernoullia* assemblage because the latter name has a prior synonym that is a malvaceous angiosperm (Bombacaceae)] (32), “Northern China” continental floristic province whereas the Badaowan (Early Jurassic) floras belong to the *Coniopters–Phoenicopsis* or “Siberian” continental floristic province, both of which are typical northern-hemisphere, high-latitude humid assemblages. The transition between the *Danaeopsis–Symopteris* and *Coniopters–Phoenicopsis* assemblages around the Triassic–Jurassic transition is interpreted as indicating a transition to more humid

and warm conditions (13). Generally, warm and humid conditions in both formations are consistent with the broad-leaf gymnosperm assemblage and the presence of common coal and are consistent with many sedimentary basins in the early Mesozoic northern-hemisphere high latitudes (33, 34) although they clearly represent nonanalog communities and although it is very difficult to assess whether these assemblages have any time significance.

In contrast, the numerical ages of the ETE are now well-understood at 201.564 ± 0.015 Ma (30), the Triassic–Jurassic boundary between 201.32 ± 0.13 Ma and 201.39 ± 0.14 Ma (35) [mean of 201.36 ± 0.14 Ma, rms error], and the Hettangian–Sinemurian boundary at about 199.46 ± 0.17 Ma (corrected from the original 199.43 ± 0.10 Ma date of ref. 36), based on zircon $^{206}\text{Pb}/^{238}\text{U}$ ages and astrochronology, with varying degrees of precision and additional uncertainty (up to 0.1%) due to very slightly different interlaboratory methods. The duration of the Hettangian is thus now well-established, with the most recent estimates being 2 My (U-Pb; ref. 37), 1.8 My (astrochronology; refs. 31, 38, and 39), and 1.88 ± 0.16 My (U-Pb; refs. 30 and 36). These durations are all close to the duration of 2 My for the Hettangian in the most recent timescale compilation (40). Based on the U-Pb dates and astrochronology in ref. 30, we used the last appearance of *L. rhaeticus* to tie the Badaowan section at 201.50 ± 0.1 Ma (Figs. 2 and 3 and Fig. S3).

Analytical Methods. The FFT and MTM spectra (Fig. 4 and Figs. S4 and S5) were developed using Analyseries (2.0) (41), and the evolutive wavelet spectrum was computed using the Matlab script of Torrence and Compo (42) (paos.colorado.edu/research/wavelets/). For all data, the original depth series was interpolated with an increment of 0.1 m. Data were divided into two series: a low LITH index series with values from 20 to 60, which were then reversed

and rescaled to range from 0 to 40 (with 40 being fine grained and 0 being coarse), and a high LITH index series with values from 60 to 140 (with 60 being fine grained and 140 being coarse). For the MTM spectra the following Analyseries options were used: linear trend was removed, medium confidence vs. resolution was selected, width.ndata product was 4, six windows were used, output was resampled from 0 to 2 with a step of 0.001, and inferior and superior error bars and amplitude spectra were computed (for Fig. 4 and Fig. S4). For the FFT, periodograms (power spectra) were prepared with the following Analyseries options: linear trend was removed, Bartlett window was used, and output was resampled from 0 to 2 with a step of 0.001. Note that Analyseries does not use adaptive weighting and thus tends to overestimate the number of significant harmonics in frequencies with low power. Consequently, we regarded only cycles with high power and high f-test statistics as having been meaningful. For the 405-ky filtered clipped-LITH data, a frequency of 0.0289855 m per cycle was used with a bandwidth of 0.005, with a Gaussian shape. For the 405-ky frequency of the total organic carbon (TOC) data of ref. 38, a frequency of 0.00062486 cm per cycle was used with a bandwidth of 0.0003 and a Gaussian shape. The modulation of obliquity (Fig. S7) is based on bandpass filtering the clipped LITH series with a 0.275 m per cycle frequency and a bandwidth of 0.02 and a Gaussian shape, which was then demodulated [amplitude modulated (AM) filtered]. The result was compared with a bandpass filtering of the clipped LITH series at a frequency of 0.0142857 m per cycle and a bandwidth of 0.01 and a Gaussian shape. The wavelet spectra were computed using the Matlab script of Torrence and Compo (42) (paos.colorado.edu/research/wavelets/software.html) with $dt = 0.1$ and all other options at the default values.

- Paleomap Project. Available at www.globalgeology.com/. Accessed February 26, 2015.
- Scotese CR, Moore TL, Dreher CT (2013) Teaching and research tools for deep time studies: Ancient Earth app, Global Geology website, and the PALEOMAP PaleoAtlas for ArcGIS. *GSA Abstracts with Programs* 45:233.
- Scotese CR (2013) *PALEOMAP PaleoAtlas for ArcGIS, Jurassic & Triassic* (PALEOMAP Project, Evanston, IL), Vol 3.
- Kent DV, Tauxe L (2005) Corrected Late Triassic latitudes for continents adjacent to the North Atlantic. *Science* 307(5707):240–244.
- Choulet F, et al. (2013) First Triassic palaeomagnetic constraints from Junggar (NW China) and their implications for the Mesozoic tectonics in Central Asia. *J Asian Earth Sci* 78:371–394.
- Tauxe L (2005) Inclination flattening and the geocentric axial dipole hypothesis. *Earth Planet Sci Lett* 233:27–261.
- Tauxe L, Kodama KP, Kent DV (2008) Testing corrections for paleomagnetic inclination error in sedimentary rocks: A comparative approach. *Phys Earth Planet Inter* 169:152–165.
- Carroll AR, Graham SA, Smith ME (2010) Walled sedimentary basins of China. *Basin Res* 22(1):17–32.
- Ashraf AR, et al. (1999) The Triassic–Jurassic boundary in the Junggar Basin (NW China): Preliminary palynostratigraphic results. *Acta Palaeobotanica* 1999(Suppl 2):85–91.
- Ashraf AR, Wang X, Sun G, Li J, Mosbrugger V (2001) Palynostratigraphic analysis of the Huangshanjie-, Haojiagou- and Badaowan formations in the Junggar Basin (NW China). *Proceedings of the Sino-German Cooperation Symposium on Paleontology, Geological Evolution and Environmental Changes of Xinjiang, China* (Jilin University, Ürümqi, China), pp 40–64.
- Ashraf AR, Sun Y-W, Li J, Sun G, Mosbrugger V (2004) Palynostratigraphic analysis of the Huangshanjie-, Haojiagou-, Badaowan-, Sangonghe- and Xishanyao Formation (Upper Triassic–Middle Jurassic) in the Southern Junggar Basin (NW China). *Proceedings of the Sino-German Cooperation Symposium on Paleontology, Geological Evolution and Environmental Changes of Xinjiang, China, Ürümqi*, eds Sun G, Mosbrugger V, Ashraf AR, Sun YW (Jilin University, Ürümqi, China), pp 41–44.
- Ashraf AR, et al. (2010) Triassic and Jurassic palaeoclimate development in the Junggar Basin, Xinjiang, northwest China: A review and additional lithological data. *Palaeobiodivers Palaeoenviro* 90(3):187–201.
- Sun G, Mosbrugger V, Miao Y-Y, Ashraf AR (2010) The Upper Triassic to Middle Jurassic strata and floras of the Junggar Basin, Xinjiang, Northwest China. *Palaeobiol Palaeoenviro* 90(3):203–214.
- Hornung J, Hinderer M (2011) Depositional dynamics and preservation potential in a progradational lacustrine fluvio-deltaic setting: Implications for high-resolution sequence stratigraphy (Upper Triassic, Northwestern China). *From River to Rock Record: The Preservation of Fluvial Sediments and Their Subsequent Interpretation*, eds Davidson SK, Leleu S North CP (SEPM Society for Sedimentary Geology, Tulsa, OK), SEPM Special Publication No. 97, pp. 281–310.
- Sha J, et al. (2011) The stratigraphy of the Triassic–Jurassic boundary successions of the southern margin of Junggar Basin, northwestern China. *Acta Geol Sin* 85(2): 421–436.
- Sha J, et al. (2012) *Type-Boundary Section of Non-Marine Base-Jurassic and Regional Correlation: Research Report Establishing Stages of Major Dates in China*, ed The Third National Stratigraphical Committee of China (Geological Publishing House, Beijing), pp 148–159. In Chinese.
- Sha J, et al. (2010) Astronomical calibrated time intervals for the non-marine Badaowan Formation, Lower Jurassic in Haojiagou of Ürümqi City, Western China. *Earth Sci Front* 17(Special Issue):22–23.
- Deng S, et al. (2010) *The Jurassic System of Northern Xinjiang, China* (University of Science and Technology of China Press, Hefei, China).
- Xu D, Ji X, Ceng X, Luo Z (2000) Study of high resolution continental cyclostratigraphy: Example of Badaowan Formation in Haojiagou, Xinjiang. *Proceedings of the Third National Stratigraphical Conference of China* (Geological Publishing House, Beijing), pp. 191–196. In Chinese.
- Vajda V, Bercovici A (2014) The global vegetation pattern across the Cretaceous–Paleogene mass extinction interval: A template for other extinction events. *Global Planet Change* 122:29–49.
- Bomfleur B, McLoughlin S, Vajda V (2014) Fossilized nuclei and chromosomes reveal 180 million years of genomic stasis in royal ferns. *Science* 343(6177):1376–1377.
- Weiss M (1989) Die Sporenfloren aus Rät und Jura Südwest-Deutschlands und ihre Beziehung zur Ammoniten-Stratigraphie. *Palaeontographica B* 215:1–168.
- Page KN, et al. (2000) East Quantoxhead, Somerset: A candidate global stratotype section and point for the base of the Sinemurian Stage (Lower Jurassic). *GeoResearch Forum* 6:163–171.
- Bloos G, Page KN (2002) Global stratotype section and point for base of the Sinemurian Stage (Lower Jurassic). *Episodes* 25(1):22–28.
- Kürschner WM, Hergreen GFW (2010) Triassic palynology of central and north-western Europe: A review of palynofloral diversity patterns and biostratigraphic subdivisions. *Geol Soc Lond Spec Publ* 334:263–283.
- Bonis NR, Kürschner WM (2012) Vegetation history, diversity patterns, and climate change across the Triassic/Jurassic boundary. *Paleobiology* 38(2):240–264.
- Mander L, Kürschner WM, McElwain JC (2013) Palynostratigraphy and vegetation history of the Triassic–Jurassic transition in East Greenland. *J Geol Soc London* 170:37–46.
- Cirilli S, et al. (2009) Latest Triassic onset of the Central Atlantic Magmatic Province (CAMP) volcanism in the Fundy Basin (Nova Scotia): New stratigraphic constraints. *Earth Planet Sci Lett* 286(3–4):514–525.
- Bonis NR, Ruhl M, Kürschner WM (2010) Milankovitch-scale palynological turnover across the Triassic–Jurassic transition at St. Audrie's Bay, SW UK. *J Geol Soc London* 167:877–888.
- Blackburn TJ, et al. (2013) Zircon U-Pb geochronology links the end-Triassic extinction with the Central Atlantic Magmatic Province. *Science* 340(6135):941–945.

31. Whiteside JH, Olsen PE, Eglinton T, Brookfield ME, Sambrotto RN (2010) Compound-specific carbon isotopes from Earth's largest flood basalt eruptions directly linked to the end-Triassic mass extinction. *Proc Natl Acad Sci USA* 107(15):6721–6725.
32. Kustatscher E, Pott C, van Konijnenburg-van Cittert JHA (2011) A contribution to the knowledge of the Triassic fern genus *Symopteris*. *Rev Palaeobot Palynol* 165(1):41–60.
33. Lu B, Deng S, Qi X (2000) Jurassic climatic events of North China and their geological significance. *GeoResearch Forum* 6:463–472.
34. Willis KJ, McElwain JC (2002) *The Evolution of Plants* (Oxford Univ Press, New York).
35. Wotzlaw J-F, et al. (2014) Towards accurate numerical calibration of the Late Triassic: High-precision U-Pb geochronology constraints on the duration of the Rhaetian. *Geology* 42:571–574.
36. Guex J, et al. (2012) Geochronological constraints on post-extinction recovery of the ammonoids and carbon cycle perturbations during the Early Jurassic. *Palaeogeogr Palaeoclimatol Palaeoecol* 346–347:1–11.
37. Schaltegger U, Guex J, Bartolini A, Schoene B, Ovtcharova M (2008) Precise U-Pb age constraints for end-Triassic mass extinction, its correlation to volcanism and Hettangian post-extinction recovery. *Earth Planet Sci Lett* 267:266–275.
38. Ruhl M, et al. (2010) Astronomical constraints on the duration of the early Jurassic Hettangian stage and recovery rates following the end-Triassic mass extinction (St. Audrie's Bay/East Quantoxhead, UK). *Earth Planet Sci Lett* 295:262–276.
39. Olsen PE, Kent DV, Whiteside JH (2011) Implications of the Newark Supergroup-based astrochronology and geomagnetic polarity time scale (Newark-APTS) for the tempo and mode of the early diversification of the Dinosauria. *Earth Environ Sci Trans R Soc Edinburgh* 101:201–229.
40. Gradstein FM, Ogg JG, Schmitz M, Ogg G, eds (2012) *The Geologic Time Scale 2012* (Elsevier Science, Oxford).
41. Paillard D, Labeyrie L, Yiou P (1996) Macintosh program performs time-series analysis. *Eos Trans AGU* 77:379.
42. Torrence C, Compo GP (1998) A practical guide to wavelet analysis. *Bull Am Meteorol Soc* 79:61–78.
43. Maron M, et al. (2015) Magnetostratigraphy of the Pignola-Abriola section: new constraints for the Norian/Rhaetian boundary. *Geol Soc Am Bull*, 10.1130/B31106.

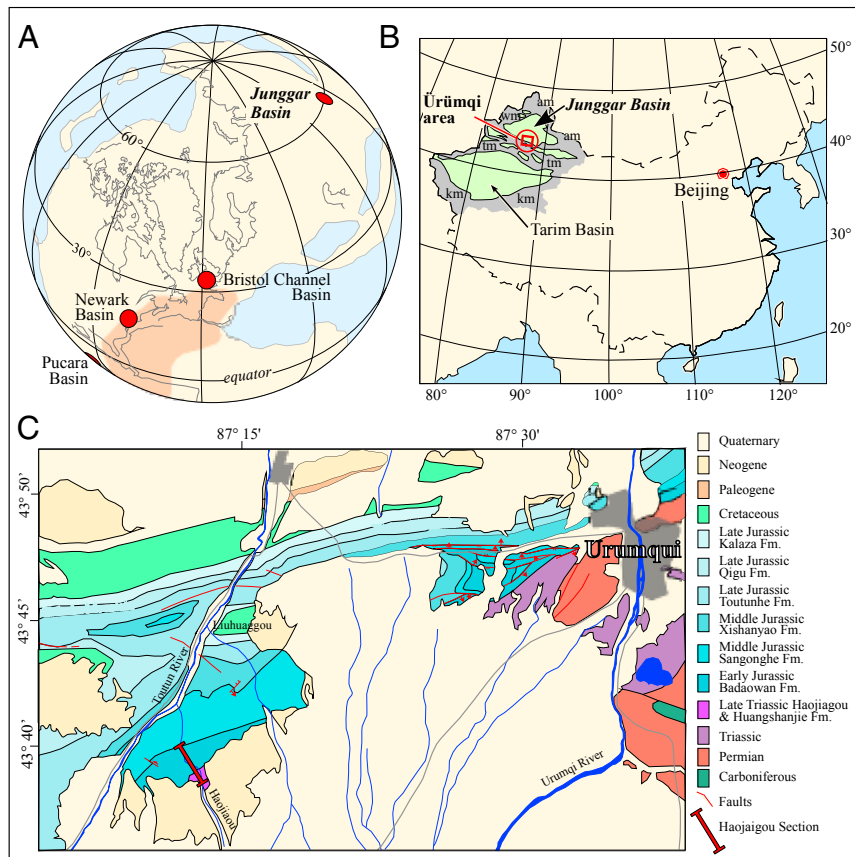


Fig. S1. Paleogeographic and present position of the Junggar Basin. (A) Paleogeographic position of the Junggar Basin, Bristol Channel, Newark–Hartford, and Pucara basins with the distribution of the Central Atlantic Magmatic Province shown in darker tan. (B) Map of the Junggar and Tarim basins, Northwest China (based on ref. 8). as, Altay Shan; ks, Kunlun Shan; ts, Tian Shan. (C) Map of the surficial geology of the Ürümqi area showing the position of the Haojiagou section.



Fig. S2. Images of the Junggar Basin section. (A) GoogleEarth image of Haojiagou section (red box), the location of which is shown in Fig. S1, showing relatively undeformed strata tilting to the north-northeast. (B) Photograph of portion of the Haojiagou section including beds 45–53, looking west across the valley. The section was measured on the east side of Haojiagou from where the photograph was taken.

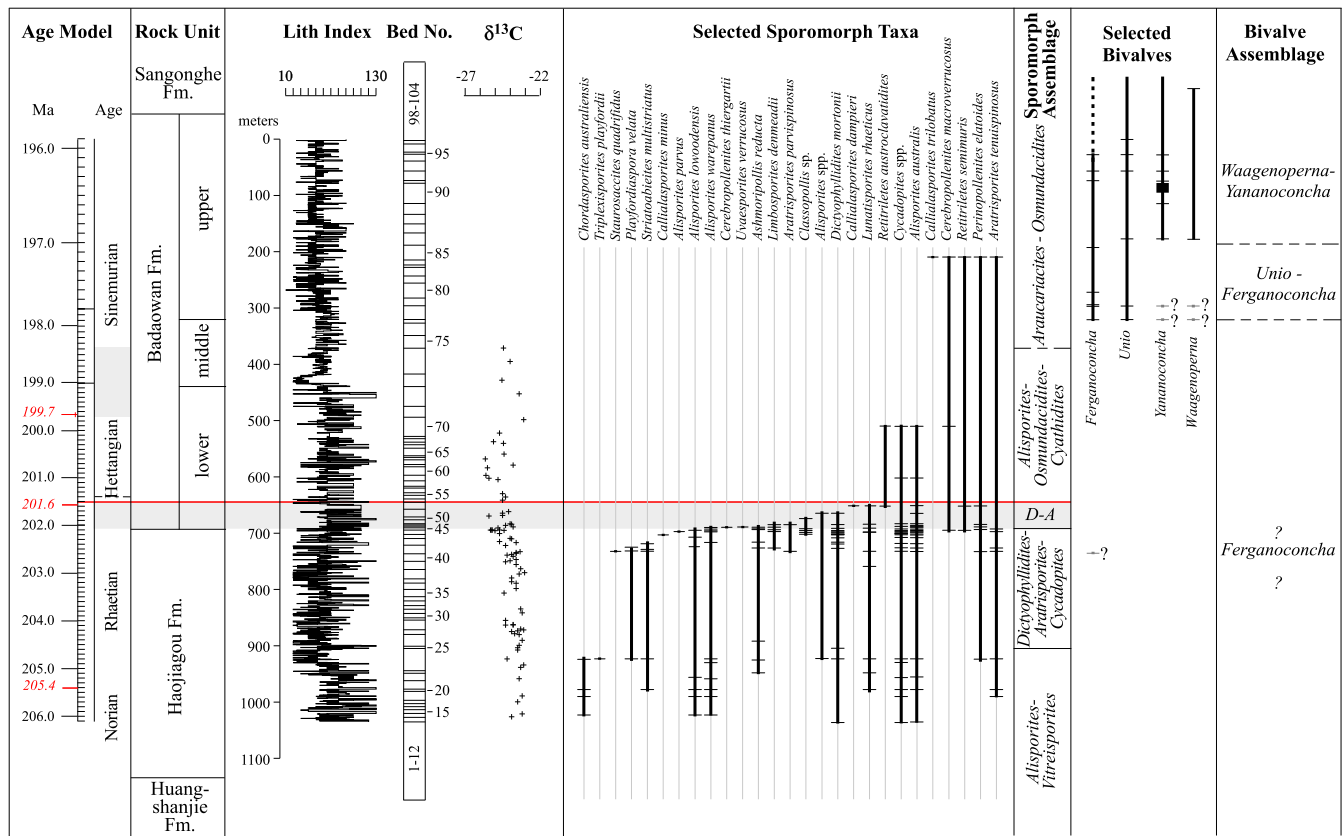


Fig. S3. Measured LITH index, simplified stratigraphic column, bed numbers, biostratigraphic data, and age model for the Haojiagou section. The occurrences of taxa are shown by ticks based on new counts, on which the new sporomorph assemblages are based. The red line marks the top of the range of *L. rhaeticus* in our studied section, the marker taxon used to correlate the lower Badaowan Formation to the eastern North American and United Kingdom sections (Fig. 4). The numerical ages in the age model are based on recognition of the 405-ky cycle in the MTM spectra, with the ages indicated in red representing the projections into the section of the initial end-Triassic extinction (201.6 Ma) and the Hettangian–Sinemurian boundary (199.7 Ma; thicker red bar indicated uncertainty from Fig. 4), and the Norian–Rhaetian boundary date is based on the Newark–Hartford APTS (interpreted by ref. 43) and the independent $^{206}\text{Pb}/^{238}\text{U}$ zircon Pucara Basin ashes (35). Gray fill in the standard ages indicates the range of possible boundary picks internal to data from the Junggar Basin itself, and the dashed lines indicate stage boundaries as suggested in ref. 17. The $\delta^{13}\text{C}$ data are from ref. 33. All data are registered to the bed numbers as measured by this field party in the Haojiagou section.

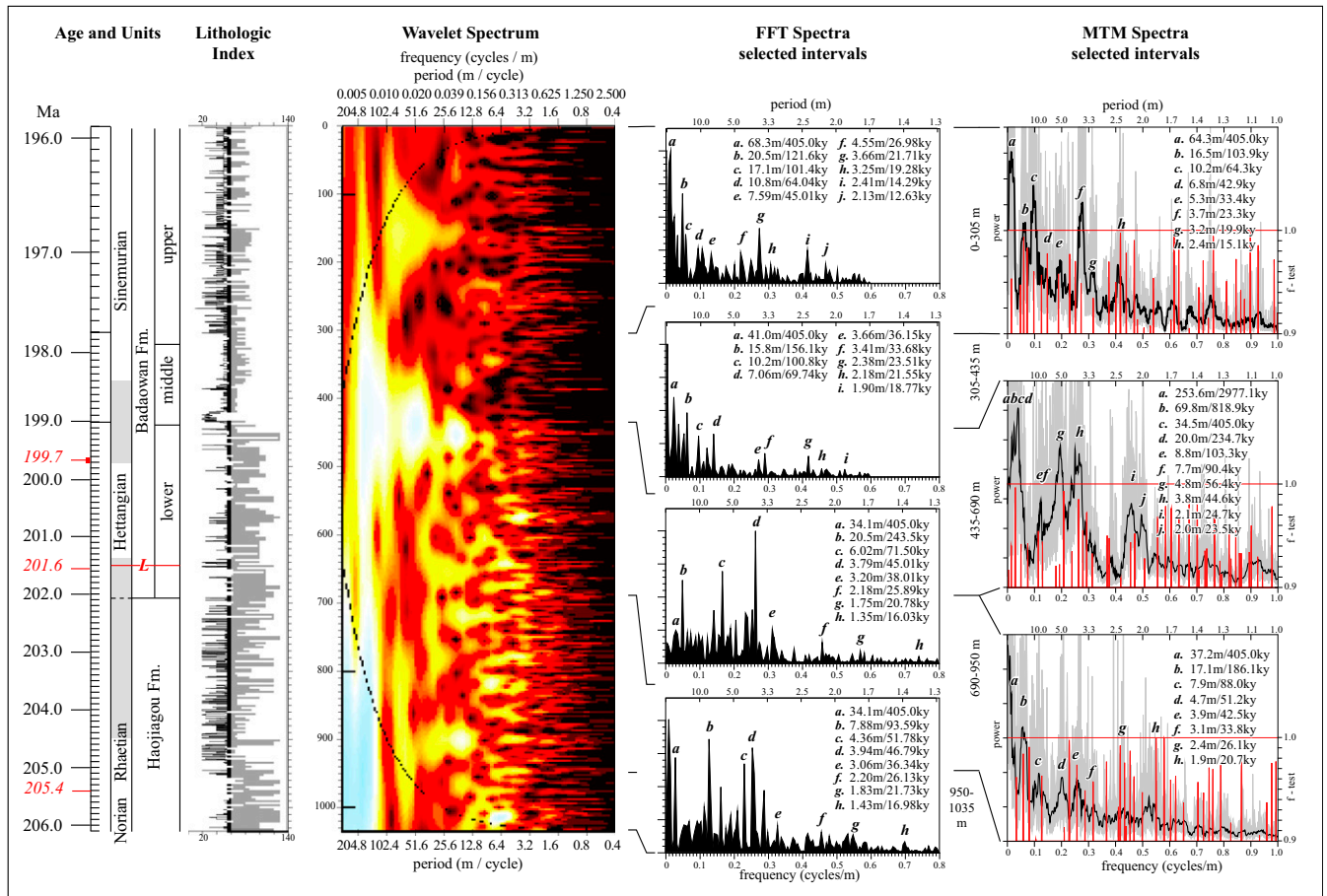


Fig. S4. Wavelet spectrum, FFT, and MTM spectral results from the clipped LITH scale (grayed part clipped off) of the upper part of the Haojiagou Formation through the upper member of the Badaowan Formation in the Haojiagou section. Conventions for temporal information are as in Fig. S3. In the evolutive FFT, white is the highest relative power and black is the lowest. In the FFT spectra, high-amplitude peaks are labeled with their periods in meters and ky (kiloyears) assuming recognition of the 405-ky cycle. In the MTM spectra, only those peaks in spectral power that have f-test significance above the 0.9 level and high amplitude are labeled, and they are labeled in meters and kiloyears based on recognition of the 405-ky level.

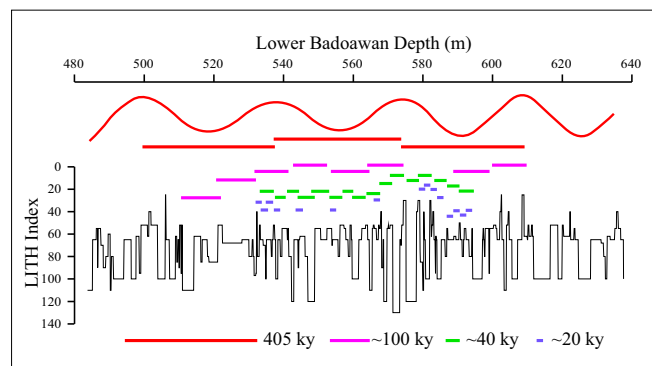


Fig. S7. The various major cycles discussed in this paper as they appear in the LITH index.

Table S1. LITH index values (rock colors range from black to light gray)

Lithology	Environment	LITH value
Coal or coal seam	Dysoxic sediment-starved lake or swamp	10
Shale, carbonaceous shale	Dysoxic lake	25
Mudstone	Shallow lake	30
Silty mudstone	Shallow lake	40
Muddy siltstone	Shallow lake or paleosol	50
Fine-grained siltstone	Shallow lake or paleosol	55
Medium-grained siltstone	Floodplain or paleosol	60
Coarse-grained siltstone	Floodplain or paleosol	65
Fine-grained sandstone	Floodplain and fluvial	70
Fine-grained sandstone	Fluvial	80
Medium-grained sandstone	Fluvial	90
Coarse-grained sandstone	Fluvial	100
Fine conglomerate: ≤ 4 -cm clasts	Fluvial	110
Medium conglomerate: ≤ 8 -cm clasts	Fluvial	120
Coarse conglomerate: > 8 -cm clasts	Fluvial	130

Table S2. U-Pb and astrochronological ages compared: Explanation

Horizon or unit	Newark igneous U-Pb	Newark–Hartford APTS	Pucara Basin U-Pb	Bristol Channel Basin Pucara*/Newark [†]
Hettangian–Sinemurian boundary	Not applicable	199.70 \pm 0.02	199.46 \pm 0.17 [‡]	199.61/199.66
Hook Mountain Basalt	200.916 \pm 0.064 [§]	200.93 \pm 0.02	Not applicable	Not applicable
Preakness Basalt	201.274 \pm 0.032 [¶]	201.28 \pm 0.02	Not applicable	Not applicable
Rhaetian–Hettangian boundary	Not applicable	201.42 \pm 0.02	201.36 \pm 0.14 [#]	201.32/201.37
Orange Mountain Basalt	201.520 \pm 0.034	201.52 \pm 0.02 ^{**}	Not applicable	Not applicable
End–Triassic extinction	201.564 \pm 0.015 ^{††}	201.56 \pm 0.02 ^{**}	201.51 \pm 0.15	201.51/201.56

*Using the Pucara ash-based ETE as a tie point (35).

[†]Using the Newark igneous-based ETE as a tie point (30).

[‡]Zircon ²⁰⁶Pb/²³⁸U age of Pucara Basin ash LM4-19B at the Hettangian–Sinemurian boundary, originally published as 199.43 \pm 0.1 Ma (15) but adjusted here to 199.46 \pm 0.17 based on a regression of ages of ashes dated by both Guex et al. (36) and Wotzlaw et al. (35), the latter using updated EARTHTIME protocols (www.earth-time.org). B. Schoene (pers. comm., 02/15) has recalculated this age using current EarthTime protocols as 199.51 \pm 0.10.

[§]Zircon ²⁰⁶Pb/²³⁸U age of the Butner Diabase that applies to the Hook Mountain Basalt (30).

[¶]Zircon ²⁰⁶Pb/²³⁸U age of flow 2 of the Preakness Basalt (30).

[#]Average age and rms error of marine Pucara Basin ashes LM4-100/101 and LM4-90 zircon ²⁰⁶Pb/²³⁸U ages that bracket the ammonite-calibrated Triassic–Jurassic boundary (35).

^{||}Zircon ²⁰⁶Pb/²³⁸U age of the Palisade Sill that applies to the Orange Mountain Basalt (30).

^{**}Age of the Triassic–Jurassic boundary as projected into the Newark APTS (31).

^{††}Age of the continental ETE in the basins of Eastern North America and Morocco derived from zircon ²⁰⁶Pb/²³⁸U dates and astrochronology (30).

^{**}Rounded age of the continental ETE (30) used as a tie point for the Newark astrochronology.